Published by Avanti Publishers

Journal of Chemical Engineering Research Updates

ISSN (online): 2409-983X

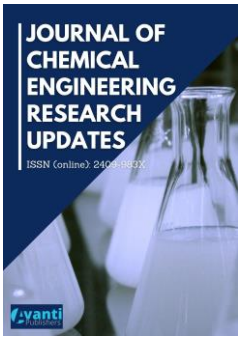

Plasma-Assisted Fenton Oxidation of Sulfadoxine in Water: Kinetics, Reactive Species Evolution, Transformation Pathways, and Ecotoxicity Assessment

Panagiotis A. Bizirtsakis[1], Konstantinos Kourtzanidis[1], Kyriaki Anagnostopoulou[2,3], Dimitrios C. Sioutopoulos[1], Dimitra A. Lambropoulou[2,3], Panagiotis Dimitrakellis[1] and Konstantinos V. Plakas[1,*]

[1]*Chemical Process & Energy Resources Institute CPERI, Centre for Research & Technology Hellas (CERTH), Thermi, Thessaloniki, Greece*

[2]*Department of Chemistry, Aristotle University of Thessaloniki, Thessaloniki, Greece*

[3]*Centre for Interdisciplinary Research and Innovation (CIRI-AUTH), Balkan Center, Thessaloniki, Greece*

ARTICLE INFO

Article Type: Research Article

Academic Editor: Meng He

Keywords:
Non-Thermal Plasma (NTP)
Plasma-Fenton hybrid process
Sulfonamide antibiotic degradation
Transformation products (TPs) & ecotoxicity
Reactive Oxygen and Nitrogen Species (RONS)

Timeline:
Received: April 16, 2026
Accepted: July 01, 2026
Published: July 14, 2026

Citation: Bizirtsakis PA, Kourtzanidis K, Anagnostopoulou K, Sioutopoulos DC, Lambropoulou DA, Dimitrakellis P, Plakas KV. Plasma-assisted Fenton oxidation of sulfadoxine in water: Kinetics, reactive species evolution, transformation pathways, and ecotoxicity assessment. J Chem Eng Res Updates. 2026; 13: 1-18.

DOI: https://doi.org/10.15377/2409-983X.2026.13.1

*Corresponding Author
Email: kplakas@certh.gr
Tel: +(30) 2310 498185

ABSTRACT

Non-thermal plasma (NTP) has emerged as a promising, electrified technology for the degradation of pharmaceutical pollutants in wastewater. In this study, ambient air NTP was employed to degrade sulfadoxine (SDX), a sulfonamide antibiotic, using a pin-to-water dielectric barrier discharge (DBD). Plasma treatment alone achieved complete SDX degradation within 45 minutes, with only 33% mineralization after 90 minutes. To enhance performance, a hybrid plasma-assisted Fenton process was developed by introducing Fe^{2+} ions, enabling total SDX removal in just 20 minutes and achieving 33% mineralization in 30 minutes. The hybrid system also reduced nitrate (NO_3^-) accumulation by over 75% compared to plasma alone. Long-lived reactive species including H_2O_2, NO_2^-, and NO_3^- were quantified over treatment time. High-resolution mass spectrometry (HRMS) identified six transformation products (TPs), four of which are reported for the first time contributing new mechanistic insight into plasma-based sulfonamide degradation pathways. These were primarily formed through desulfonation, aromatic bond cleavage, and hydroxylation pathways. In silico ecotoxicity screening using ECOSAR revealed that several TPs were as toxic or more toxic than the parent compound, particularly under chronic exposure to aquatic organisms. These results underline the effectiveness and relevance of plasma/Fenton processes for the treatment of sulfonamide-contaminated water, while also highlighting the need for ongoing assessment of TPs' toxicity.

1. Introduction

Water pollution has emerged as a prominent research field, due to the escalating ecological pressure coming from the increased human activity. The active compounds of the pharmaceutical products, such as antibiotics, are among the greatest contributors to this issue. The widespread usage of antibiotics has resulted in their pervasive presence within the environment, inflicting considerable harm upon aquatic ecosystems [1-4]. The profoundly toxic nature of these compounds, even at minimal concentrations, has aroused the necessity for extensive research over their environmental fate [5, 6]. Sulfadoxine (SDX), a sulfonamide used for the treatment of malaria, has gained significant attention from regulatory bodies due to the looming risks associated with the development of antibiotic resistance [7-9]. This has aroused the necessity for the development of novel water treatment technologies, spurring the exploration of Advanced Oxidation Processes (AOPs) as a promising and environmental-friendly approach for degrading persistent organic pollutants. [10-13]. The core principle of AOPs is the generation of oxidative hydroxyl radicals (·OH) that can react, effectively and non-selectively with all the organic pollutants in water [10, 11, 14, 15].

Recent advancements in AOPs have proposed the use of non-thermal plasma (NTP) as a green, electrified alternative [16-20]. While NTP is known for generating a broad range of reactive oxygen and nitrogen species (RONS), its mechanisms of antibiotic degradation, the nature of transformation products formed, and their ecotoxicity implications remain underexplored. Recent studies have expanded on this, showing that atmospheric plasma discharges produce a wide spectrum of reactive oxygen and nitrogen species that contribute to both oxidative and nitrosative degradation of contaminants [21, 22]. NTPs in air-rich atmosphere are capable of generating reactive oxygen and nitrogen species (RONS) with varying oxidative potential [23, 24] and are thus a promising technology for water treatment [25, 26]. Short-lived species (e.g. $^{\bullet}OH^{-}$, $^{\bullet}O_2^{-}$ and $^{\bullet}HOO$), produced by plasma systems exhibit high reactivity, triggering mechanisms that lead to the degradation and transformation of organic contaminants [27]. Despite their brief lifespan, hydroxyl radicals emerge as the dominant species within this system, typically oxidizing the majority of organic compounds present in the aqueous solution, while also engaging in recombination reactions to form H_2O_2 [28, 29]. In addition to hydroxyl chemistry, plasma–water systems generate nitrogen-based radicals (e.g., NO_2·, NO^+, N_2O_5), which may participate in side reactions such as nitrosation under acidic conditions [30, 31]. The long-lived RONS formed in water upon interaction with air plasmas, i.e., e.g., H_2O_2, NO_2^- and NO_3^-, generally exhibit mild reactivity. H_2O_2 does not react with organic pollutants directly but serves as a valuable source of hydroxyl radicals when acting synergistically with other reagents, catalysts, or radiation [32]. Furthermore, NO_x species have been observed to interact with organic species, initiating transformative mechanisms [24, 26, 33, 34]. The generation of hydroxyl radicals, alongside secondary RONS, underscores the potential of plasma-assisted AOPs [21, 35-40]. Notably, the absence of additional reagents or produced waste in plasma-based processes indicate the green character of such systems [41-43].

Fenton process represents one of the most commonly employed AOPs in the wastewater treatment field due to its conceptual simplicity and modest equipment requirements [44-46]. However, it presents notable limitations, such as the generation of substantial quantities of chemical sludge (iron sediment) and increased consumption of chemicals like H_2O_2 and acids for pH adjustment [44]. Recent efforts have proposed hybrid plasma-assisted Fenton systems as a way to address these limitations, leveraging plasma-generated H_2O_2 and HNO_3 to sustain radical production and maintain acidic conditions without external dosing [38, 47-51]. Despite these promising developments, most studies to date have focused on model dyes or general organics, with limited exploration into pharmaceutical pollutants, especially sulfonamides, and scarce attention to mechanistic insights, transformation product formation, or ecotoxicity implications.

While AOPs offer significant benefits in terms of degrading target contaminants, achieving total mineralization (removal of Total Organic Carbon, TOC) is often limited. This limitation is indicative of the formation of secondary intermediates known as Transformation Products (TPs), which are categorized as emerging contaminants [52-54]. It is typically assumed that TPs are less toxic than the parent compound, although this isn't always the case [55, 56]. Given the promising potential of plasma-assisted applications, it is important to elucidate the mechanism of degradation, as well as the toxic potential of generated TPs, from such processes. This aspect has been

investigated extensively in various organic contaminants, including sulfonamides, with a range of mechanisms reported, including hydroxylation, bond cleavage, oxidation, reduction, and nitration [57-60].

In this study, we delve into the efficacy of NTP in degrading SDX, exploring various operational parameters of NTP including the kinetics of long-lived RONS such as H_2O_2, NO_2^- and NO_3^-. Additionally, we significantly enhance the process efficiency, targeting higher degradation rates and improved mineralization, while mitigating the presence of dissolved N-containing compounds in treated samples, by employing a synergistic Fenton reaction through a hybrid plasma-assisted Fenton oxidation process. Furthermore, we conducted an investigation into the degradation mechanisms, which involved identifying 6 TPs, 4 of which are reported for the first time filling the research gap of occurring transformation mechanisms. To assess the ecotoxicity (both acute and chronic) of the generated TPs on fish, daphnids and green algae organisms, we employed a Quantitative Structure-Activity Relationship (QSAR) software named ECOSAR. Thus, this study aims to fill the gap in mechanistic understanding by investigating the detailed transformation pathways and ecotoxicological risks associated with plasma-based and plasma/Fenton SDX degradation. The identification of four novel transformation products, the time-resolved analysis of long-lived RONS, and insights into potential nitrosation pathways distinguish this work from earlier studies and contribute to the responsible development of AOP-based treatment systems.

2. Methods

2.1. Standards, Reagents and Chemicals

An analytical grade standard (>95%) of Sulfadoxine was supplied by Supelco, USA. For the experiments, synthetic samples of 5 mg/L SDX were employed, in ultrapure water (18.2 MΩ × cm) from a purification system (MilliQ, Millipore, USA). $FeSO_4 \cdot 7H_2O$ supplied by Sigma-Aldrich, USA, was used for the Fenton related experiments, with a concentration of 2.6 mg/L $FeSO_4 \cdot 7H_2O$. For the HPLC mobile phases, HPLC grade Water and Methanol were supplied by Merck, Germany.

2.2. Plasma Processing and Diagnostics

The plasma treatment of aqueous solutions was conducted in ambient air using a non-thermal, dielectric barrier discharge (DBD) plasma reactor with a pin-to-water configuration (Fig. **1**). The aqueous solutions (100 ml) were placed inside a cylindrical glass container of 100 mm diameter that was positioned on top of a stainless-steel grounded electrode, while a pin electrode connected to a high-voltage (HV) power supply was facing the water surface. The glass bottom along with the water medium serve as the dielectric barriers and the electrode gap was fixed at 20 mm. The electrode gap here is defined as the distance between the pin's tip and the grounded electrode. The discharge gap i.e. the distance between the pin's tip and the water surface is approximately 4 mm.

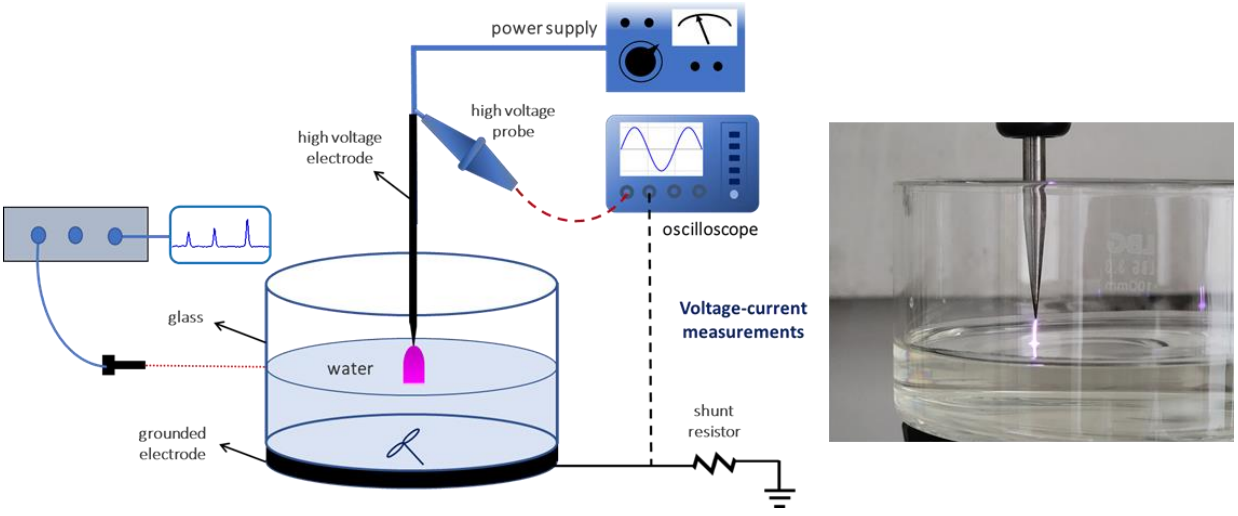

Figure 1: Experimental set-up for plasma processing of the aqueous solutions of sulfadoxine.

The plasma was generated by supplying sinusoidal AC high-voltage signals (PVM500) of around 6 kV peak-to-peak at a fixed frequency of 19.4 kHz. The voltage and current signals were recorded using a high-voltage probe (TT-HPV 2739, Testec) and a shunt resistor (1 kΩ), respectively. The signals were monitored via a Rigol DS2202A digital oscilloscope. The discharge power was calculated from the product of the time-dependent voltage v(t) and current i(t) integrated over one period (T). Optical emission spectroscopy (OES) measurements were performed using a wideband UV-Vis-NIR spectrometer (FR-Mini, ThetaMetrisis) connected to a 400 μm optical fiber adjusted to a 25 mm collimating lens.

To prevent localized oxidation at the discharge site, continuous stirring was applied.

2.3. Instrumental Analysis

Sulfadoxine was determined using a CBM-20A HPLC (Shimadzu Europa GmbH, Germany), coupled to a Diode Array detector set at 215 nm. For the analysis, a Shim-pack GIST C18 reverse phase column, 5 μm, 150 x 4.0 mm (Shimadzu, Japan), was employed similar to previous work [61]. For the detection and identification of Sulfadoxine TPs, a Q Exactive™ Focus Orbitrap LC-MS/MS (Thermo Fisher Scientific, Germany), was used as described in a previous study [52]. The H_2O_2 concentration was determined using the iodide method [62], while the NO_x species concentration was measured spectrometrically using Nitrate Test kit method (109713, Superlco, USA). For the Total Organic Carbon (TOC) measurements, a TOC-5000A Analyzer system (Shimadzu Europa GmbH, Germany) was utilized. The limit of detection (LOD) of the analysis was 0.1 mg/L. For the Total Nitrogen (TN) measurements, a TOC-L Analyzer system (Shimadzu Europa GmbH, Germany) was utilized. The LOD of the analysis was 0.02 mg/L. Prior to HPLC, TOC and TN analysis, all samples were filtered with Nylon syringe 0.22 μm filters supplied by LabSolutions, Greece. The pH and electrical conductivity of the samples were measured with a digital pH-meter (InoLab 750, WTW). No additional preservation measures were taken after sampling, as samples were analyzed by HPLC within minutes of collection. Furthermore, a previous study [61] demonstrated that SDX does not degrade in the presence of H_2O_2 alone, in the absence of UV light. To minimize light exposure, dark-colored sampling vials were used during the process.

2.4. Toxicity Assessment

For the acute and chronic toxicity assessment of the generated TPs across three trophic levels (fish, daphnids, and green algae), the software ECOSAR v2.2 (Ecological Structure Activity Relationships) was employed. The molecular structures of the TPs were input using the SMILES notation. Acute toxicity was assessed on the basis of LC50/EC50 values generated by the program, while chronic toxicity was assessed on the basis of Chronic values (ChV). Toxicity levels provided ranged from 0.0 to >100, categorizing substances as (i) very toxic (0.0-1.0), (ii) toxic (1-10), (iii) harmful (10-100), or (iv) non-toxic (>100). The approach of this analysis was based on previously reported studies [52, 61, 63, 64].

2.5. Statistical Analysis

After normalizing all values to their respective t_0, we used a two-tailed unpaired t-test assuming unequal variances (Welch's t-test) to compare groups at each time point (excluding t_0, where no variance remained).

3. Results and Discussion

3.1. Plasma Characterization

Characteristic voltage and current waveforms for the conditions applied herein are shown in Fig. (**2a**). A stable discharge is generated at applied voltages around 6 kV_{p-p}. For these conditions, the calculated discharge power ranges between 9 and 10 W, as the plasma properties slightly change over time (see below). Consistent with the detailed analysis of [65], the discharge current exhibits a strong peak during the positive-going and rising phase of the AC cycle, when the pin electrode is acting as an anode. A filamentary microdischarge is clearly visible, bridging the discharge gap and forming an anode spot at the liquid interface, which has been already attributed to the accumulation of surface charges at the dielectric (liquid) interface [66]. The plasma spreading at this interface, has

also been observed in DBDs involving solid dielectrics [67]. We note here that we follow the convention of [68], where a streamer (cathode or anode directed) discharge is denoted as a propagating ionization front which transits to a non-equilibrium microdischarge or filamentary discharge upon impact to the dielectric (or electrode) surface. The maximum current corresponding to the positive microdischarge formation is around 250 mA. During the negative-going phase of the AC waveform (pin acting as cathode), we note that there is no sharp current peak, which suggests a less intense discharge formation during this phase and under the specific experimental conditions. Similar observations for the negative going cycle have been reported in [65]. A small current jump (to negative current values) occurs very close to the voltage reversal time-instant, which indicates that surface charges accumulating on the liquid surface strongly alter the potential distribution and trigger the reversal of charged species drift even at very low applied voltage. Such current signal reversal has been observed in various DBD configurations and it is typically seen in surface-DBDs [69-71] where the dielectric material is heavily charged under each sub-cycle. We note here that the complex plasma spatiotemporal dynamics inside the AC cycle which involve plasma-dielectric-liquid interaction phenomena, play a vital role in the overall balance of active species and their diffusion inside the liquid. Moreover, the water activation by the plasma-induced effects (modifying water conductivity, surface tension etc) can in turn modify the plasma properties leading to the alteration of electrostatic potential distribution, species fluxes in the gas-liquid interface and electron energy levels [72]. Electrohydrodynamic phenomena (which also are affected by the transient plasma-liquid system behavior) can also modify the plasma properties due to the induced deformation of the liquid surface, leading to a non-constant discharge gap during plasma treatment [73]. Such detailed analysis of plasma transient properties and mutually interactions between unsteady plasma and water properties is outside the scope of the current work but it explains the unsteady behavior of the discharge power during the various treatment times.

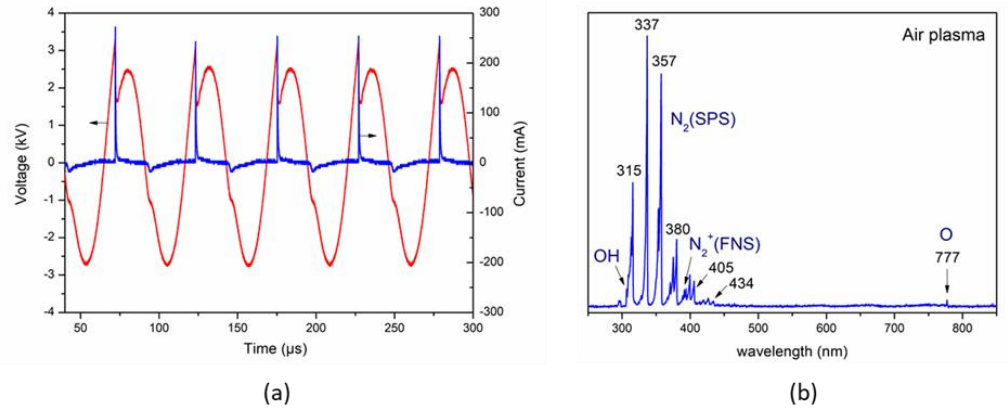

Figure 2: (a) Voltage-current signals of the plasma discharge. (b) Optical emission spectrum of the air plasma in contact with aqueous solutions of SDX.

To complement the plasma characterization, we report on the characteristic emission spectrum of the air plasma, which is presented in Fig. (**2b**). The spectrum is typical of air plasmas in contact with water [74, 75]. The emission spectrum is dominated by the peaks related to the N_2 Second Positive System (SPS) that corresponds to the $C^3\Pi_u \rightarrow B^3\Pi_g$ electronic transition with several vibrational bands ($\Delta v = v' - v''$) appearing at 315 nm ($\Delta v = +1$), 337 nm ($\Delta v = 0$), 357 nm ($\Delta v = -1$), 380 nm ($\Delta v = -2$), 405 nm ($\Delta v = -3$), and 434 nm ($\Delta v = -4$) [76, 77]. The N_2^+ First Negative System (FNS) corresponding to the transition $B^2\Sigma_u^+ \rightarrow X^2\Sigma_g^+$ with $\Delta v = 0$ is also visible at 391 nm. Despite the low intensity compared to N_2 SPS bands, the line ratio of 391/337 is still quite significant, indicative of the high reduced electric field that is typical of DBDs [78]. The OH(A-X) molecular band in the 306–309 nm range is detected as well but its signal overlaps with the N_2(C-B) transitions near 315 nm. However, its presence is still indicating a high density of OH radicals that play a major role in the oxidation reactions taking place in the gas-liquid interface. Considering also that the optical emission spectroscopy measurements are space averaged, we can expect a much higher OH contribution to the emission intensity near the water surface [74]. The peak appearing at 777 nm is attributed to the atomic oxygen transition ($3p^5P\text{-}3s^5S^0$). The low intensity of atomic oxygen band is also characteristic of the air plasma emission spectra at atmospheric pressure where the main depopulation mechanism of excited atomic oxygen species is through quenching with N_2 and O_2, with radiative processes being much less significant [18].

3.2. Plasma and Plasma/Fenton oxidation

OES analysis reveals a rich plasma chemistry, typical of air discharges that generate a multitude of gaseous reactive oxygen and nitrogen species (RONS). The plasma generated RONS interact with the liquid water and cause further reactions in the gas-liquid interface and in the bulk liquid [79]. Among the dominant reactive oxygen species that are implicated to oxidative reactions with organic molecules in the liquid phase are the hydroxyl radicals (·OH) and hydrogen peroxide (H_2O_2). The former are short-lived species produced mostly in the gas-phase via electron impact dissociation of water molecules that escape the liquid (R1) and they are rapidly quenched (upon collisions with other species in the plasma) or absorbed in the liquid water where they can directly interact with organic molecules or recombine towards formation of H_2O_2 (R2) [28, 80, 81]. The stable (long-lived) H_2O_2 can also be formed through recombination of ·OH radicals in the gas-phase and subsequently absorbed in the liquid. H_2O_2 is accumulated in the liquid phase and despite its limited reactivity with sulfadoxine, it is critical in the Fenton process for its activation towards ·OH. An important aspect in the case of ·OH diffusion in the liquid is that the SDX oxidation and the H_2O_2 formation are competing reactions that both consume ·OH radicals.

$$e^- + H_2O \rightarrow \cdot H + \cdot OH + e^- \text{ (R1)}$$

$$\cdot OH + \cdot OH \rightarrow H_2O_2 \text{ (R2)}$$

As the plasma processing takes place in open air, several N-containing reactive species are also formed in the plasma and interact with the liquid water as well. NO species are initially formed in the plasma following several pathways, from the Zeldovich to the direct oxidation of atomic nitrogen upon interaction with O and OH radicals [74, 82, 83]. NO can be further oxidized towards higher oxides. The NOx species can also interact with ·OH both in the gas and liquid phase leading to the formation (and absorption) of nitrous (HNO_2) and nitric (HNO_3) acid. Such species participate in further interactions in the bulk liquid that lead to formation of other RONS (e.g., ONOOH), water acidification, and also possible interactions with the organic molecules [80, 84, 85].

The main long-lived RONS that accumulate in the plasma treated aqueous solutions of SDX, i.e., H_2O_2, NO_2^- and NO_3^- were measured and the evolution of their concentration as a function of the plasma processing time is presented in Fig. (**3**). A simultaneous increase in H_2O_2 and NO_2^- concentration is observed for the first 10 min of plasma treatment. The concentration of NO_2^- steadily decreased after 10 min till total elimination after 60 min, while H_2O_2 showed a rapid increase till 40 min and then rapidly decreased. This drop in the concentration of H_2O_2 and NO_2^- may be partially explained by their mutual interaction at low pH values leading to the formation of peroxynitrous acid (ONOOH) [82, 86]. Other degradation mechanisms are also possible considering the complex pathways incorporating the organic molecules (SDX and transformation products). In contrast, NO_3^- generation is constantly increasing almost linearly throughout the entire process, reaching concentration levels as high as 250 mg/L after 90 minutes.

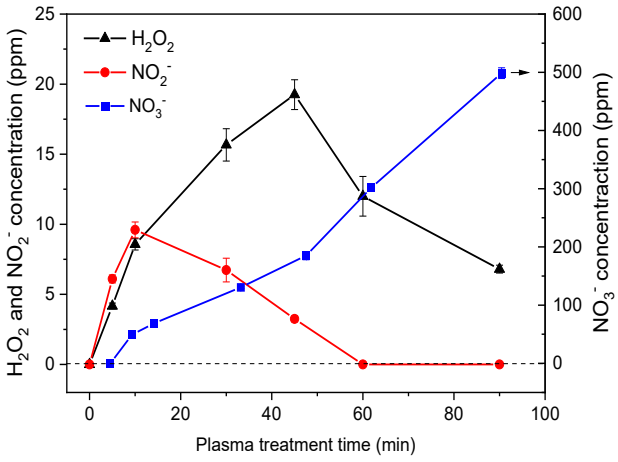

Figure 3: Concentration of long-lived reactive oxygen and nitrogen species in aqueous SDX solutions as a function of plasma treatment time.

In the Plasma/Fenton process, no NO_3^- was detected after 20 min processing. After that point, their concentration increased, reaching a level of 55.5 mg/L after 30 minutes. This observation can be elucidated by considering the interactions between iron complexes and the produced anions. In Fenton systems, iron species tend to form complexes, and their surface becomes charged based on the pH [87-89]. Under acidic conditions, negative species become adsorbed on the surface of these complexes, inhibiting their availability in the solution [87, 90]. The sharp increase in dissolved NO_3^- between the 20 and 30 min treatment can be attributed to the saturation of ferric complexes under the specific conditions. This is further supported by the presence of H_2O_2 after 30 minutes of processing (Table **1**), as saturation with NO_3^- can impede the activation of H_2O_2 by the catalyst [87].

Table 1: Concentrations of long-lived RONS (NO_3, NO_2 and H_2O_2) in aqueous SDX solutions at different plasma treatment durations in the plasma/Fenton process.

Time (min)	NO_3^- conc (mg/L)	NO_2^- conc (mg/L)	H_2O_2 conc (mg/L)
0	<0.4	<0.5	<0.1
20	<0.4	2.1 ± 0.5	<0.1
30	55.5 ± 2.6	14.0 ± 1.1	3.2 ± 0.2

TN measurements confirmed that nitrogen was not fully mineralized during the treatment period, consistent with the accumulation of NO_3^- and NO_2^- and species quantifies in Fig. (**3**) and Table **1**. The incomplete TN balance suggests the possible formation of small nitrogenous transformation products (e.g. nitriles, amines etc.), that fall below the detection capabilities threshold of HRMS.

The formation of RONS in the plasma-treated liquid induces alterations to the conductivity and pH of the solution (Table **2**). In the plasma process, the formation of NOx ionic species leads to drastic increase in the water conductivity, from 7 μS/cm for the SDX solution in MilliQ water to >1600 μS/cm after 90 min of treatment. The acidic species, mainly HNO_3, are responsible for the rapid drop in the pH (lower than pH 3 after 30 min). The same trend is observed in the plasma/Fenton process, with the increase of conductivity and corresponding drop of the pH being more pronounced. The initial conductivity of these solutions was higher, due to the presence of the $FeSO_4$ salt, affecting the discharge behavior at the initial stages and causing alterations to the kinetics of RONS species. It should be noted that Fe^{2+} was introduced as a one-time reagent at t=0 rather than as a catalytic species. Under the acidic conditions generated by the plasma, Fe^{2+} is progressively oxidized to Fe^{3+}, which may precipitate as iron hydroxide upon pH neutralization post-treatment. Given the low Fe^{2+} concentration employed (2.6 mg/L $FeSO_4{\cdot}7H_2O$), however, sludge generation remains minimal compared to conventional Fenton processes, while the enhancement in degradation efficiency and NOx mitigation justifies its use at this concentration.

Table 2: Electrical conductivity and pH alteration with plasma treatment time in the plasma and plasma/Fenton processes.

Time (min)	pH	E. Conductivity (μS/cm)
Plasma		
0	5.4	7
30	2.9	446
60	2.7	980
90	2.4	1625
Plasma / Fenton		
0	4.4	227
20	2.6	550
30	2.5	733

The absence of detectable H_2O_2 at 20 min in the plasma/Fenton process, despite the simultaneous presence of NO_2^- at 2.1 mg/L, can be attributed not only to the expected rapid Fenton reaction kinetics, but also to the limitation that a short but finite interval between collection and measurement is present, leading to any residual H_2O_2 present at the moment of sampling to be further consumed during this period, falling below the LOD of the iodide method. The transient accumulation of NO_2^- at this timepoint is consistent with the early-stage plasma chemistry, prior to its subsequent consumption via interaction with H_2O_2 and acidic species as described above.

Both the RONS and the ·OH radicals actively interact with the SDX, resulting in its transformation. According to the RONS kinetics, H_2O_2 was rapidly produced even in the starting minutes of the simple plasma process. H_2O_2 does not directly react with SDX, meaning that its accumulation in the treated solution acts as a scavenging effect, reducing the degradation rates. Total removal of SDX is achieved after 45 min. As depicted in Fig. (**4**), the plasma/Fenton process turned out to be superior, with total removal being achieved in only 20 min of treatment. These can be attributed to the activation of the formed H_2O_2, resulting in the increase of oxidative ·OH radicals in the solution.

A kinetic analysis of SDX degradation showed that it followed pseudo-first-order kinetics in both NTP and NTP/Fenton processes. For the NTP process, a rate constant of k_NTP = 0.040 min^{-1} (R^2 = 0.929, t½ = 17.2 min) was obtained over the treatment period (t = 0–30 min). The NTP/Fenton process yielded a significantly higher rate constant of k_Fenton = 0.263 min^{-1} (R^2 = 0.953, t½ = 2.6 min), corresponding to an enhancement factor of 6.5 relative to the NTP process alone. This enhancement is consistent with the activation of plasma-generated H_2O_2 by Fe^{2+} via the Fenton reaction, which substantially increases the ·OH radical concentration available for SDX oxidation. Notably, the NTP/Fenton degradation profile exhibited a biphasic character, with an initial rapid phase in which approximately 70% of SDX was removed within the first 2 minutes of treatment (Fig. **4**). This burst is attributed to the availability of Fe^{2+} in excess of the initially plasma-generated H_2O_2, enabling an intense Fenton reaction. As Fe^{2+} is progressively oxidized to Fe^{3+} and depleted below a critical threshold, the process transitions to a rate governed by the availability of plasma-generated H_2O_2, consistent with the pseudo-first-order behavior observed from t = 2 min onward.

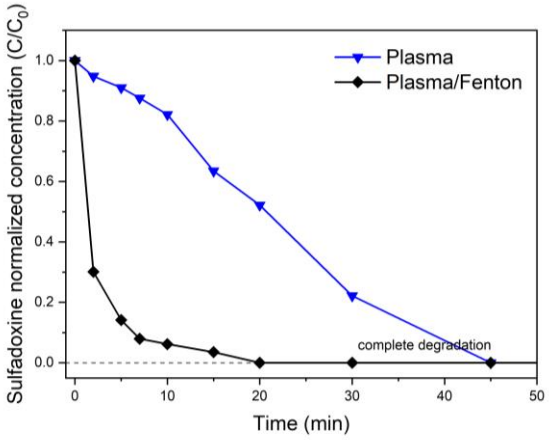

Figure 4: Normalized concentration (C/C_0) of SDX as a function of plasma treatment time for both simple NTP and NTP/Fenton processes.

The energy efficiency of both processes was evaluated using the Electrical Energy per Order (EEO) figure-of-merit, as defined by Bolton *et al*. [91] for batch systems operating under pseudo-first-order kinetics (Eq. 1):

$$EEO = 38.4 \cdot P / (V \cdot k) \quad \text{Eq. 1}$$

where P is the rated power [kW], V is the treated volume [L], and k is the pseudo-first-order rate constant [min^{-1}]. Using P = 9.5 W (average discharge power), V = 0.1 L, and the experimentally determined rate constants, the EEO values were calculated as 90.7 kWh/m^3/order for the NTP process and 13.9 kWh/m^3/order for the NTP/Fenton process, representing an 84.7% reduction in energy demand upon addition of Fe^{2+}. These values are consistent

with the range reported in the literature for plasma-based degradation of sulfonamide antibiotics (EEO values of 22.4 and 7.5 kWh/m³/order have been reported for NTP degradation of sulfamethazine and sulfathiazole respectively under comparable DBD conditions) confirming that the hybrid plasma/Fenton approach offers a meaningful improvement in energy efficiency over plasma-only systems, while remaining within the performance range of optimized plasma-AOP configurations for this class of contaminants [92].

Despite the complete removal of the contaminant in both plasma systems, mineralization rates, as presented in Table **3**, were notably slower. Specifically, 90 min were required in order to remove 33% of the TOC content in the simple plasma process, whereas the hybrid plasma/Fenton system achieved the same rate in just 30 min, a behaviour aligned with letarature discussions [93, 94]. Interestingly, substantial mineralization rates seemed to occur only following the complete degradation of SDX, in both systems.

Table 3: Mineralization rates as obtained by Total Organic Carbon (TOC) measurements at different plasma treatment durations in the plasma and plasma/Fenton processes.

Time (min)	TOC (C/C_0)
Plasma	
0	1
30	0.98
60	0.8
90	0.67
Plasma / Fenton	
0	1
20	0.89
30	0.67

All statistical comparisons were conducted using a two-tailed unpaired t-test assuming unequal variances (Welch's t-test) after normalization to the initial concentration, with all post-t_0 differences found to be significant ($p < 0.001$, ranging from 5.27×10^{-7} to 4.21×10^{-5}; detailed results in Supplementary Information, Table **S1**).

3.3. SDX Transformation Products

Since achieving total mineralization was not feasible despite the complete degradation of SDX, the identification of the generated transformation products using Orbitrap HRMS could provide valuable insights into the existing degradation mechanisms.

Prior research has been done in investigating certain degradation pathways of SDX through photocatalytic, solar photolysis and microbial treatment methods [61, 95, 96]. However, only 2 of the total 6 identified transformation products (TPs) generated from NTP have previously been reported. This suggests that distinct mechanisms occur in a NTP-assisted process, resulting in entirely different intermediate pathways.

SDX's MS^2 spectra fragmentation mechanisms are presented in Fig. (**5**), corroborating previously published data [61]. These results play a crucial role in identifying the detected TPs.

As presented in Fig. (**6**), a total of 6 TPs were identified, indicating distinct mechanism of formation. It is proposed that their generation involves the combination of 3 main transformation mechanisms, desulfonation, bond cleavage and hydroxylation. The proposed mechanisms have already been reported in a study involving heterogeneous photocatalysis [61], suggesting that such mechanisms primarily arise from the interaction between SDX and hydroxyl radicals.

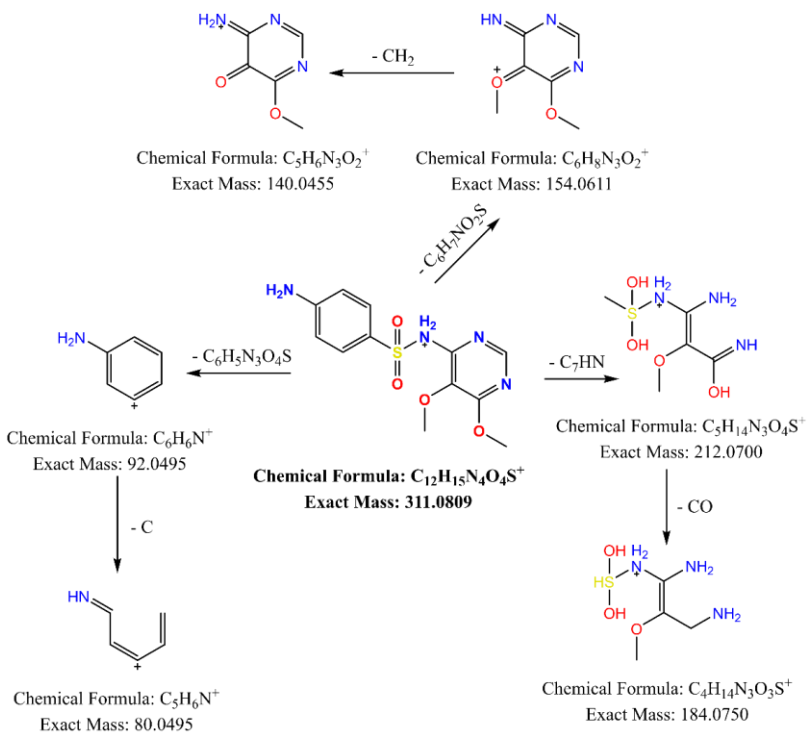

Figure 5: Proposed mechanism for the oxidative fragmentation of sulfadoxine.

However, plasma generates a broader range of RS beyond just hydroxyl radicals, with significantly more intense generation rate. The harsh conditions that were formed, due to the interaction of various oxidative ions with SDX, could lead to more rapid degradation pathways, further explaining the limitations in detecting more TPs, as explained in the following paragraphs.

3.3.1. Desulfonation

The mechanism of desulfonation has been previously reported for SDX, along with the TP247 ($C_{12}H_{15}N_4O_2^+$, m/z = 247,1190) [61]. In that work, TP247 was one of the major species that were generated, in contrast to the NTP's case. In this work, TP247 was detected in traces, the signal intensity associated with this TP was insufficient to trigger a fragmentation. One likely explanation, is that the TP247 follows 2 different transformation pathways, and transforms rapidly into secondary products.

3.3.2. Bond Cleavage

Bond cleavage is one of the most typical transformation mechanisms observed in AOPs. In the case of sulfadoxine, such mechanism can take place in the main S-N bond, forming the major product, TP156 ($C_6H_{10}N_3O_2^+$, m/z = 156.0769), which has also been previously reported in all of the cases involving SDX [61, 95, 96]. TP235 ($C_6H_{11}N_4O_4S^+$, m/z = 235.0494) seems to occur following the cleavage of aromatic bonds. This type of transformation seems to be possible when oxygen based radicals attack the aromatic ring, destabilizing its bonds and eventually opening. In similar cases, where this is reported [97-99], variety of groups like alcohols or aldehydes are generated, which seems to be the case in the TP235. Specifically, 2 hydroxyl groups are added to the structure, but due to the presence of this TP in trace concentration levels, the collection of fragmentation data was not possible. Accordingly, TP235 is tentatively identified based on accurate mass measurement only, and its exact structural assignment remains to be confirmed.

3.3.3. Hydroxylation

Despite, being the most expected mechanism to be observed, the TPs of the hydroxylated-SDX product, was not detected, like it did in the case of heterogeneous photocatalysis [61]. In contrast, intense hydroxylation seemed to occur on the structure of TP247, unlocking 2 separate pathways.

One of these pathways leads directly to the formation of TP248 ($C_{12}H_{14}N_3O_3^+$, m/z = 248.1034), the least abundant of the major TPs. Its formation involves the removal of the amine from the aniline ring, followed by a hydroxyl group is addition on one of the ring's carbons.

The second pathway includes 2 TPs, the TP277 ($C_{12}H_{13}N_4O_4^+$, m/z = 277.0935) which is tentatively identified based on accurate mass only, as its trace-level presence precluded fragmentation, and the TP293 ($C_{12}H_{13}N_4O_5^+$, m/z = 293.0885), which was the dominant TP of this process. TP293 seems to occur by the simple attachment of an additional hydroxyl group on the TP277's structure, allowing the later's structure confirmation based on the structure of TP293. The MS^2 fragmentation data for TP293 are available in Supplementry information (Table **S2**), however, the observed fragment ions do not allow unambiguous assignment of the hydroxylation site on the TP293's structure. Interestingly, the highly oxidative conditions led to the addition of aldehyde groups, without causing aromatic ring opening, like in other reported cases [97].

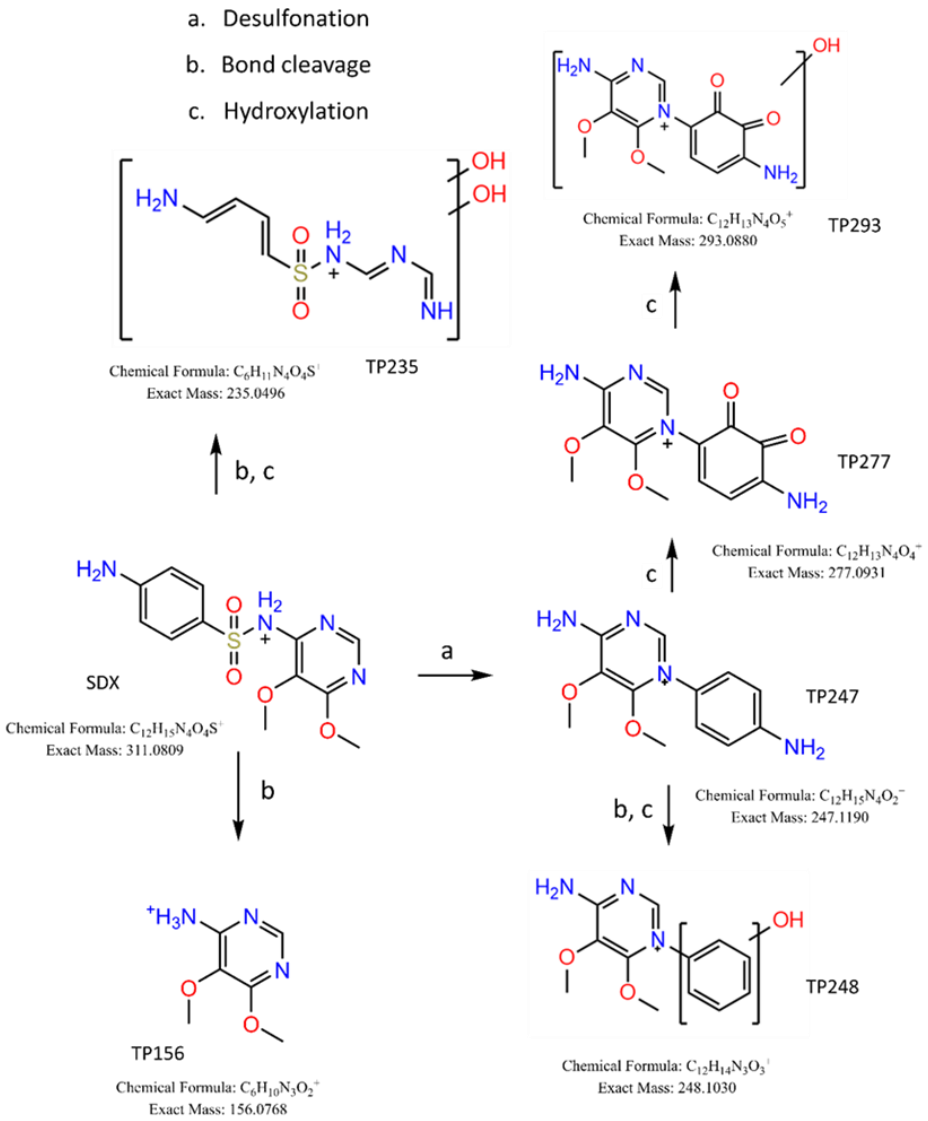

Figure 6: Proposed transformation mechanism of SDX using plasma treatment. The mechanisms include a) Desulfonation, b) Bond cleavage, and c) Hydroxylation.

3.4. Evaluation of TP Time Profiles

As mentioned in the previous paragraphs, the conditions developed in this process were highly reactive, leading to distinct, but rapid transformation pathways, meaning that only few of the TPs dominated the overall

abudance, while the rest stayed in in trace levels. In order to further understand this behavior, along with the general degradation mechanism of SDX, it is important to study the time profiles of these TPs. In order to quantify the generated molecules, that are not commercially available, a semi-quantification approach was utilized, similarly to previously published cases [52, 61]. By recording the changes in peak areas, over time, we managed to track the abundance of these species. Specifically, in Fig. (**7**), the time profiles of TP156, TP248 and TP293 are visualized. Interestingly, their relative peak areas are observed between 15 to 20 minutes after the beginning of the process, while they are not detected anymore after 60 minutes.

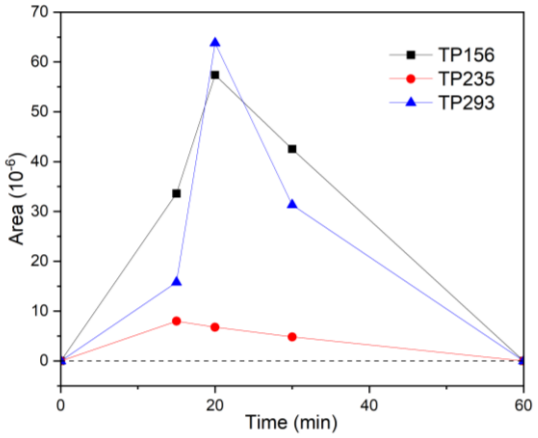

Figure 7: Time profiles of the dominant transformation products. Time profiles were constructed using the raw chromatographic peak areas of each transformation product and are indicative of temporal abundance trends, as no internal standard was used, for semi-quantification.

3.5. In Silico Assessment of TPs' Ecotoxicity Using ECOSAR

Given that main purpose of AOPs is the protection of the environment, the toxicity of the emerged TPs should be assessed, as part of the process's evaluation. The ECOSAR software provides a valuable tool for *in silico* assessment of pollutants' ecotoxicity, based on their structure. Both acute and chronic toxicity on three different aquatic organisms (Fish, Daphnide and Green algae) were estimated based on criteria established by European Union (No. 1272/2008/EC) [100], similarly to previously published studies [52, 61, 96]. This analysis was based on the mathematical relationship between the relative log value of the estimated toxicity (mmol/L), which translates to the concentration of a substance at which a particular effect (50% mortality) is observed. Additionally, the logK_{ow} values, are also predicted with these models (EPI Suite KOWWIN prediction). As explained in paragraph 2.4, the toxicity levels ranged from 0.0 to >100, classifying substances as (i) very toxic (0.0-1.0), (ii) toxic (1-10), (iii) harmful (10-100), or (iv) non-toxic (>100) (Fig. **8**). The complete numerical LC50/EC50 and chronic value (ChV) predictions for all compounds are provided in Supplementary Information (Table **S3**).

SDX's ecotoxicity when it behaves as an aniline in the environment, was already reported, as mostly concerning towards daphnides, in long term exposure [61]. TP156 and TP247, both classified as anilines by ECOSAR, have been previously reported in the context of SDX degradation [61]. TP156 was classified as non-toxic across all organisms and exposure durations (Fish LC50 = 7.53×10^{6} mg/L, Daphnid LC50 = 2.62×10^{6} mg/L), consistent with the loss of the sulfonamide and aniline moieties upon ring-opening reducing biological activity. TP247 exhibited similar toxicity to SDX, with a slightly elevated daphnid chronic toxicity (ChV = 0.086 mg/L vs. 0.12 mg/L for SDX), remaining in the very toxic category for daphnids under long-term exposure.

TP235, resulting from aromatic bond cleavage and ring opening, was classified as non-toxic across all three trophic levels and both acute and chronic exposure scenarios (Fish LC50 = 1.83×10^{5} mg/L, Daphnid LC50 = 1.15×10^{4} mg/L, Algae EC50 = 3.37×10^{4} mg/L). The disruption of the aniline and diazine rings appears to substantially reduce the biological activity of this compound, representing a toxicologically favorable transformation pathway.

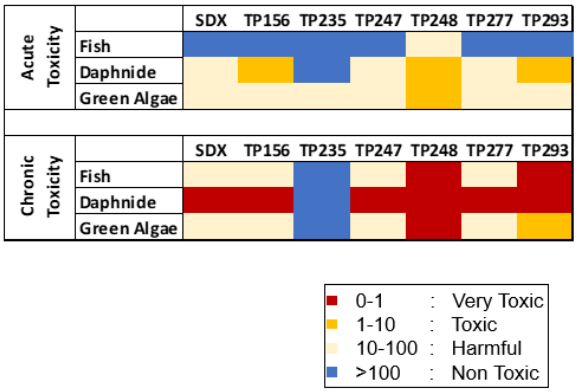

Figure 8: Toxicity assessment of SDX TPs, generated from NTP treatment, using in silico tool ECOSAR.

Desulfonation was the main mechanism observed in this process. According to previous reports, TPs generated from the transformation of desulfonation products, tent to exhibit various levels of toxicity, lacking behaviour patterns [61]. In this work, the TPs originating from TP247 appeared to be equally to more toxic than SDX, without specific patterns being observed. Interestingly, despite the general reported observation of hydroxylation products being less toxic, TP248 and TP293 were the most toxic compounds of the group [101, 102]. TP248 displayed close to 44-fold greater acute fish toxicity (LC50 = 22.1 mg/L vs. 967 mg/L for SDX) and ~133-fold greater chronic fish toxicity (ChV = 0.183 mg/L vs. 24.4 mg/L for SDX). Similarly, TP293 showed 8-fold greater acute fish toxicity (LC50 = 115 mg/L) and around 35 times greater chronic fish toxicity (ChV = 0.693 mg/L) relative to SDX. For green algae, TP293 exhibited 18-fold greater chronic toxicity (ChV = 1.79 mg/L vs. 32 mg/L for SDX). These findings are particularly noteworthy given that hydroxylation products are generally assumed to be less toxic than their parent compounds [101, 102]. The present results demonstrate that this assumption does not universally hold, especially when hydroxylation introduces phenolic amine moieties with known aquatic toxicity.

TP277, was classified as an aniline by ECOSAR and exhibited very toxic chronic daphnid toxicity (ChV = 0.155 mg/L), consistent with the aniline structural class. Its toxicity profile is intermediate between SDX and the more toxic hydroxylated products TP248 and TP293.

Overall, the ecotoxicological assessment reveals that while certain transformation pathways, specifically aromatic ring opening leading to TP235, result in detoxification, the dominant hydroxylation pathway generates products of equal or greater concern than the parent antibiotic. This underscores the necessity of transformation product monitoring in plasma-based AOP systems and cautions against assuming complete detoxification upon parent compound removal.

4. Conclusions

SDX, as an emerging contaminant, has garnered increasing attention due to its widespread use in malaria treatment, raising concerns over the development of antibiotic resistance by pathogenic microorganisms. This study evaluated the degradation of the persistent sulfonamide, using NTP and a hybrid NTP/Fenton process. While both processes achieved complete SDX removal, the hybrid system significantly improved efficiency, reducing treatment time to 20 minutes and achieving 33% mineralization in just 30 minutes. It also limited the accumulation of NO_3^- in the treated water, addressing a common limitation of plasma-based methods.

A major contribution of this work is the kinetic analysis of long-lived reactive species (H_2O_2, NO_2^-, NO_3^-), which provided mechanistic insights into how plasma chemistry evolves under Fenton-enhanced conditions. High-resolution mass spectrometry enabled the identification of six TPs, four of which are reported here for the first time. Their formation was linked to specific degradation mechanisms such as desulfonation, aromatic bond cleavage, and hydroxylation.

Finally, a QSAR-based toxicity assessment revealed that several TPs exhibited equal or greater toxicity than SDX, particularly under chronic exposure. This underscores the need for transformation product monitoring in

advanced oxidation processes. Overall, this study advances the application of hybrid plasma processes for antibiotic removal and contributes new understanding of reaction pathways and environmental risks.

Conflict of Interest

The authors declare no conflict of interest.

Funding

The study received no financial support.

Acknowledgment

The work of K. Kourtzanidis and P. Dimitrakellis was funded by the European Union Project EPHYRA, supported by the Clean Hydrogen Partnership in collaboration with Hydrogen Europe and Hydrogen Europe Research under the GA number 101112220. Views and opinions expressed are however those of the author(s) only and do not necessarily reflect those of the European Union or the Clean Hydrogen Joint Undertaking. Neither the European Union nor the granting authority can be held responsible for them.

References

[1] Homem V, Santos L. Degradation and removal methods of antibiotics from aqueous matrices – A review. J Environ Manage. 2011; 92(10): 2304-47. http://doi.org/10.1016/j.jenvman.2011.05.023

[2] Okoye CO, Okeke ES, Okoye KC, Echude D, Andong FA, Chukwudozie KI, *et al*. Occurrence and fate of pharmaceuticals, personal care products (PPCPs) and pesticides in African water systems: A need for timely intervention. Heliyon. 2022; 8(3): e09143. http://doi.org/10.1016/j.heliyon.2022.e09143

[3] Zhang Z, Li X, Liu H, Zamyadi A, Guo W, Wen H, *et al*. Advancements in detection and removal of antibiotic resistance genes in sludge digestion: A state-of-the-art review. Bioresour Technol. 2022; 344: 126197. http://doi.org/10.1016/j.biortech.2021.126197

[4] Duan W, Cui H, Jia X, Huang X. Occurrence and ecotoxicity of sulfonamides in the aquatic environment: A review. Sci Total Environ. 2022; 820: 153178. http://doi.org/10.1016/j.scitotenv.2022.153178

[5] Vila-Costa M, Gioia R, Aceña J, Pérez S, Casamayor EO, Dachs J. Degradation of sulfonamides as a microbial resistance mechanism. Water Res. 2017; 115: 309-17. http://doi.org/10.1016/j.watres.2017.03.007

[6] Zhou J, Yun X, Wang J, Li Q, Wang Y. A review on the ecotoxicological effect of sulphonamides on aquatic organisms. Toxicol Rep. 2022; 9: 534-40. http://doi.org/10.1016/j.toxrep.2022.03.034

[7] Abdul-Ghani R, Farag HF, Allam AF. Sulfadoxine-pyrimethamine resistance in Plasmodium falciparum: A zoomed image at the molecular level within a geographic context. Acta Trop. 2013; 125(2): 163-90. http://doi.org/10.1016/j.actatropica.2012.10.013

[8] Chen FL, Song KH, Xu JT, Wang KZ, Feng XZ, Han GC, *et al*. An electrochemical aptamer sensor for rapid quantification sulfadoxine based on synergistic signal amplification of indole and MWCNTs and its electrooxidation mechanism. Sens Actuators B Chem. 2024; 401: 135008. http://doi.org/10.1016/j.snb.2023.135008

[9] Su Z, Wang K, Yang F, Zhuang T. Antibiotic pollution of the Yellow River in China and its relationship with dissolved organic matter: Distribution and source identification. Water Res. 2023; 235: 119867. http://doi.org/10.1016/j.watres.2023.119867

[10] Deng Y, Zhao R. Advanced oxidation processes (AOPs) in wastewater treatment. Curr Pollut Rep. 2015; 1(3): 167-76. http://doi.org/10.1007/s40726-015-0015-z

[11] Pandis PK, Kalogirou C, Kanellou E, Vaitsis C, Savvidou MG, Sourkouni G, *et al*. Key points of advanced oxidation processes (AOPs) for wastewater, organic pollutants and pharmaceutical waste treatment: A mini review. ChemEng. 2022; 6(1): 1. http://doi.org/10.3390/chemengineering6010008

[12] Rana S, Kumar A, Dhiman P, Mola GT, Sharma G, Lai CW. Recent advances in photocatalytic removal of sulfonamide pollutants from wastewater by semiconductor heterojunctions: A review. Mater Today Chem. 2023; 30: 101603. http://doi.org/10.1016/j.mtchem.2023.101603

[13] Bali M, Mbarki W, Boulanouar L. Advanced oxidation processes and treatment strategies for hospital wastewater: A comprehensive review. Eng Sci Technol. 2025; 7(1): 144-55. http://doi.org/10.37256/est.7120268992

[14] Petsi PN, Sarasidis VC, Plakas KV, Karabelas AJ. Reduction of nitrates in a photocatalytic membrane reactor in the presence of organic acids. J Environ Manage. 2021; 298: 113526. http://doi.org/10.1016/j.jenvman.2021.113526

[15] Plakas KV, Sarasidis VC, Patsios SI, Lambropoulou DA, Karabelas AJ. Novel pilot scale continuous photocatalytic membrane reactor for removal of organic micropollutants from water. Chem Eng J. 2016; 304: 335-43. http://doi.org/10.1016/j.cej.2016.06.075

[16] Cameli F, Dimitrakellis P, Vlachos DG. Direct conversion of ethane to oxygenates, ethylene, and hydrogen in a noncatalytic biphasic plasma microreactor. ACS Sustain Chem Eng. 2023; 11(21): 8003-8. http://doi.org/10.1021/acssuschemeng.3c01594

[17] Dimitrakellis P, Giannoglou M, Xanthou ZM, Gogolides E, Taoukis P, Katsaros G. Application of plasma-activated water as an antimicrobial washing agent of fresh leafy produce. Plasma Process Polym. 2021; 18(12): 2100030. http://doi.org/10.1002/ppap.202100030

[18] Walsh JL, Liu DX, Iza F, Rong MZ, Kong MG. Contrasting characteristics of sub-microsecond pulsed atmospheric air and atmospheric pressure helium-oxygen glow discharges. J Phys D Appl Phys. 2010; 43(3): 032001. http://doi.org/10.1088/0022-3727/43/3/032001

[19] Magureanu M, Mandache NB, Parvulescu VI. Degradation of pharmaceutical compounds in water by non-thermal plasma treatment. Water Res. 2015; 81: 124-36. http://doi.org/10.1016/j.watres.2015.05.037

[20] Zhang H, Deng S, Zhu L, Liu Y. Degradation of sulfamethoxazole in a falling film dielectric barrier discharge system: Performance, mechanism and toxicity evaluation. Sci Total Environ. 2024; 956: 177320. http://doi.org/10.1016/j.scitotenv.2024.177320

[21] Giardina A, Lofrano G, Libralato G, Siciliano A, Marotta E, Paradisi C. Air non-thermal plasma, a green approach for the treatment of contaminated water: The case of sulfamethoxazole. Front Environ Chem. 2024; 5: 1416702. http://doi.org/10.3389/fenvc.2024.1416702

[22] Yin Y, Xu H, Zhu Y, Zhuang J, Ma R, Cui D, *et al*. Recent progress in applications of atmospheric pressure plasma for water organic contaminants' degradation. Appl Sci. 2023; 13(23): 12631. http://doi.org/10.3390/app132312631

[23] Labay C, Hamouda I, Tampieri F, Ginebra MP, Canal C. Production of reactive species in alginate hydrogels for cold atmospheric plasma-based therapies. Sci Rep. 2019; 9(1): 16160. http://doi.org/10.1038/s41598-019-52673-w

[24] Tampieri F, Ginebra MP, Canal C. Quantification of plasma-produced hydroxyl radicals in solution and their dependence on the pH. Anal Chem. 2021; 93(8): 3666-70. http://doi.org/10.1021/acs.analchem.0c04906

[25] Takeuchi N, Yasuoka K. Review of plasma-based water treatment technologies for the decomposition of persistent organic compounds. Jpn J Appl Phys. 2020; 60(SA): SA0801. http://doi.org/10.35848/1347-4065/abb75d

[26] Ceriani E, Marotta E, Shapoval V, Favaro G, Paradisi C. Complete mineralization of organic pollutants in water by treatment with air non-thermal plasma. Chem Eng J. 2018; 337: 567-75. http://doi.org/10.1016/j.cej.2017.12.107

[27] Kehrer JP, Robertson JD, Smith CV. Free radicals and reactive oxygen species. In: McQueen CA, Ed. Comprehensive Toxicology. 2nd ed. Oxford: Elsevier; 2010. p. 277-307. http://doi.org/10.1016/B978-0-08-046884-6.00114-7

[28] Cameli F, Dimitrakellis P, Chen TY, Vlachos DG. Modular plasma microreactor for intensified hydrogen peroxide production. ACS Sustain Chem Eng. 2022; 10(5): 1829-38. http://doi.org/10.1021/acssuschemeng.1c06973

[29] Joshi AA, Locke BR, Arce P, Finney WC. Formation of hydroxyl radicals, hydrogen peroxide and aqueous electrons by pulsed streamer corona discharge in aqueous solution. J Hazard Mater. 1995; 41(1): 3-30. http://doi.org/10.1016/0304-3894(94)00099-3

[30] Wang Z, Wang X, Xu S, Zhou R, Zhang M, Li W, *et al*. Off-site production of plasma-activated water for efficient sterilization: The crucial role of high-valence NOx and new chemical pathways. Water Res. 2024; 252: 122541. http://doi.org/10.1016/j.watres.2024.122541

[31] Shaban M, Merkert N, van Duin ACT, van Duin D, Weber AP. Advancing DBD plasma chemistry: Insights into reactive nitrogen species such as NO2, N2O5, and N2O optimization and species reactivity through experiments and MD simulations. Environ Sci Technol. 2024; 58(36): 16087-99. http://doi.org/10.1021/acs.est.4c04894

[32] Targhan H, Evans P, Bahrami K. A review of the role of hydrogen peroxide in organic transformations. J Ind Eng Chem. 2021; 104: 295-332. http://doi.org/10.1016/j.jiec.2021.08.024

[33] Bosi FJ, Tampieri F, Marotta E, Bertani R, Pavarin D, Paradisi C. Characterization and comparative evaluation of two atmospheric plasma sources for water treatment. Plasma Process Polym. 2018; 15(3): 1700130. http://doi.org/10.1002/ppap.201700130

[34] Tampieri F, Giardina A, Bosi FJ, Pavanello A, Marotta E, Zaniol B, *et al*. Removal of persistent organic pollutants from water using a newly developed atmospheric plasma reactor. Plasma Process Polym. 2018; 15(6): 1700207. http://doi.org/10.1002/ppap.201700207

[35] Allabakshi SM, Srikar PSNSR, Gangwar RK, Maliyekkal SM. Application of plasma-assisted advanced oxidation processes for removal of emerging contaminants in water. In: Singh SP, Agarwal AK, Gupta T, Maliyekkal SM, Eds. New Trends in Emerging Environmental Contaminants. Singapore: Springer; 2022. p. 333-70. http://doi.org/10.1007/978-981-16-8367-1_15

[36] Farooq M, Rasheed H, Rehman NU. Efficacy of plasma enhanced advanced oxidation processes for decontamination of water containing arsenic. Plasma Chem Plasma Process. 2024; 44(1): 269-88. http://doi.org/10.1007/s11090-023-10392-1

[37] Ma S, Kim K, Chun S, Moon SY, Hong Y. Plasma-assisted advanced oxidation process by a multi-hole dielectric barrier discharge in water and its application to wastewater treatment. Chemosphere. 2020; 243: 125377. http://doi.org/10.1016/j.chemosphere.2019.125377

[38] Marković M, Jović M, Stanković D, Kovačević V, Roglić G, Gojgić-Cvijović G, *et al*. Application of non-thermal plasma reactor and Fenton reaction for degradation of ibuprofen. Sci Total Environ. 2015; 505: 1148-55. http://doi.org/10.1016/j.scitotenv.2014.11.017

[39] Takeuchi N, Ishibashi N, Sugiyama T, Kim HH. Effective utilization of ozone in plasma-based advanced oxidation process. Plasma Sources Sci Technol. 2018; 27(5): 055013. http://doi.org/10.1088/1361-6595/aac0ea

[40] Tsuchida A, Shimamura T, Sawada S, Sato S, Serpone N, Horikoshi S. In-liquid plasma: A stable light source for advanced oxidation processes in environmental remediation. Radiat Phys Chem. 2018; 147: 53-8. http://doi.org/10.1016/j.radphyschem.2018.01.028

[41] Gorbanev Y, Privat-Maldonado A, Bogaerts A. Analysis of short-lived reactive species in plasma-air-water systems: The dos and the do nots. Anal Chem. 2018; 90(22): 13151-8. http://doi.org/10.1021/acs.analchem.8b03336

[42] Pankaj SK, Wan Z, Keener KM. Effects of cold plasma on food quality: A review. Foods. 2018; 7(1): 1. http://doi.org/10.3390/foods7010004

[43] Robinson C, Stapelmann K. Plasma treating water for nitrate based nitrogen fertilizer: A review of recent device designs. Curr Opin Green Sustain Chem. 2024; 50: 100978. http://doi.org/10.1016/j.cogsc.2024.100978

[44] Collivignarelli MC, Pedrazzani R, Sorlini S, Abbà A, Bertanza G. H2O2 based oxidation processes for the treatment of real high strength aqueous wastes. Sustainability (Basel). 2017; 9(2): 244. http://doi.org/10.3390/su9020244

[45] Naumczyk J, Prokurat I, Marcinowski P. Leachates treatment by H2O2/UV, O3/H2O2, modified Fenton, and modified photo-Fenton methods. Int J Photoenergy. 2012; 2012: 909157. http://doi.org/10.1155/2012/909157

[46] Ahmed N, Vione D, Rivoira L, Carena L, Castiglioni M, Bruzzoniti MC. A review on the degradation of pollutants by Fenton-like systems based on zero-valent iron and persulfate: Effects of reduction potentials, pH, and anions occurring in waste waters. Molecules. 2021; 26(15): 4584. http://doi.org/10.3390/molecules26154584

[47] Grbić J, Mladenović D, Pavlović S, Veljović Đ, Lazović S, Đukić-Vuković A. Effect of combined non-thermal plasma/Fenton treatment on lignocellulose degradation in corn stalks. Book Abstr VIII Int Congr Eng Environ Mater Process Ind. 2023; p.154.

[48] Kim SH, Seo J, Hong Y, Shin Y, Chung HJ, An HR, *et al*. Construction of an underwater plasma and Fenton hybrid system for the rapid oxidation of organic dyes and antibiotics. J Water Process Eng. 2023; 52: 103519. http://doi.org/10.1016/j.jwpe.2023.103519

[49] Slamani S, Abdelmalek F, Ghezzar MR, Addou A. Initiation of Fenton process by plasma gliding arc discharge for the degradation of paracetamol in water. J Photochem Photobiol A Chem. 2018; 359: 1-10. http://doi.org/10.1016/j.jphotochem.2018.03.032

[50] Wahono JZ, Yusharyahya RD, Harianingsih, Saksono N. Phenol degradation by Fenton reaction in air injection using plasma electrolysis method. IOP Conf Ser Mater Sci Eng. 2020; 980(1): 012051. http://doi.org/10.1088/1757-899X/980/1/012051

[51] Bilea F, Bradu C, Cicirma M, Medvedovici AV, Magureanu M. Plasma treatment of sulfamethoxazole contaminated water: Intermediate products, toxicity assessment and potential agricultural reuse. Sci Total Environ. 2024; 909: 168524. http://doi.org/10.1016/j.scitotenv.2023.168524

[52] Anagnostopoulou K, Nannou C, Evgenidou E, Lambropoulou DA. Does climbazole instigate a threat in the environment as a persistent, mobile and toxic compound? Unveiling the occurrence and potential ecological risks of its phototransformation products in the water cycle. J Hazard Mater. 2023; 458: 131854. http://doi.org/10.1016/j.jhazmat.2023.131854

[53] Farré M, Pérez S, Kantiani L, Barceló D. Fate and toxicity of emerging pollutants, their metabolites and transformation products in the aquatic environment. TrAC Trends Anal Chem. 2008; 27(11): 991-1007. http://doi.org/10.1016/j.trac.2008.09.010

[54] Silva DB, Buttiglieri G, Farré MJ, Babić S. Transformation products of contaminants of emerging concern in water by UV-based processes. Water Pract Technol. 2023; 18(9): 2182-92. http://doi.org/10.2166/wpt.2023.129

[55] Silva AR, Martins PM, Teixeira S, Carabineiro SAC, Kuehn K, Cuniberti G, *et al*. Ciprofloxacin wastewater treated by UVA photocatalysis: Contribution of irradiated TiO2 and ZnO nanoparticles on the final toxicity as assessed by Vibrio fischeri. RSC Adv. 2016; 6(98): 95494-503. http://doi.org/10.1039/C6RA19202E

[56] Vela N, Calín M, Yáñez-Gascón MJ, Garrido I, Pérez-Lucas G, Fenoll J, *et al*. Photocatalytic oxidation of six pesticides listed as endocrine disruptor chemicals from wastewater using two different TiO2 samples at pilot plant scale under sunlight irradiation. J Photochem Photobiol A Chem. 2018; 353: 271-8. http://doi.org/10.1016/j.jphotochem.2017.11.040

[57] Corella Puertas E, Peyot ML, Pineda M, Volk K, Coulombe S, Yargeau V. Degradation of diatrizoate in a pin-to-liquid plasma reactor, its transformation products and their residual toxicity. Sci Total Environ. 2021; 782: 146895. http://doi.org/10.1016/j.scitotenv.2021.146895

[58] Kim KS, Kam SK, Mok YS. Elucidation of the degradation pathways of sulfonamide antibiotics in a dielectric barrier discharge plasma system. Chem Eng J. 2015; 271: 31-42. http://doi.org/10.1016/j.cej.2015.02.073

[59] Mu X, Wang X, Zhang Y, Liu B, Yang J. Major products and their formation and transformation mechanism through degrading UDMH wastewater via DBD low temperature plasma. Environ Technol. 2021; 42(17): 2709-20. http://doi.org/10.1080/09593330.2019.1710573

[60] Rayaroth MP, Aubry O, Rabat H, Marilleau E, Gru Y, Hong D, *et al*. Degradation and transformation of carbamazepine in aqueous medium under non-thermal plasma oxidation process. Chemosphere. 2024; 352: 141449. http://doi.org/10.1016/j.chemosphere.2024.141449

[61] Bizirtsakis PA, Anagnostopoulou K, Sarasidis VC, Petsi P, Moschona A, Plakas KV, *et al*. A comparative study of advanced oxidation processes for the removal of the antibiotic sulfadoxine from water—transformation products and toxicity. Appl Sci. 2025; 15(2): 793. http://doi.org/10.3390/app15020793

[62] Petsi P, Plakas KV, Frontistis Z, Karabelas AJ. A comparative assessment of carbonaceous electrodes with diverse interfacial properties for H2O2 electrogeneration. J Chem Technol Biotechnol. 2024; 99(4): 863-71. http://doi.org/10.1002/jctb.7589

[63] Reuschenbach P, Silvani M, Dammann M, Warnecke D, Knacker T. ECOSAR model performance with a large test set of industrial chemicals. Chemosphere. 2008; 71(10): 1986-95. http://doi.org/10.1016/j.chemosphere.2007.12.006

[64] Svedberg P, Inostroza PA, Gustavsson M, Kristiansson E, Spilsbury F, Backhaus T. Dataset on aquatic ecotoxicity predictions of 2697 chemicals, using three quantitative structure-activity relationship platforms. Data Brief. 2023; 51: 109719. http://doi.org/10.1016/j.dib.2023.109719

[65] Diamond J, Hamdan A, Profili J, Margot J. Time and space-resolved imaging of an AC air discharge in contact with water. J Phys D Appl Phys. 2020; 53(42): 425209. http://doi.org/10.1088/1361-6463/ab9f69

[66] Bruggeman P, Ribežl E, Maslani A, Degroote J, Malesevic A, Rego R, *et al*. Characteristics of atmospheric pressure air discharges with a liquid cathode and a metal anode. Plasma Sources Sci Technol. 2008; 17(2): 025012. http://doi.org/10.1088/0963-0252/17/2/025012

[67] Kourtzanidis K. Full cycle, self-consistent, two-dimensional analysis of a packed bed DBD reactor for plasma-assisted CO2 splitting: spatiotemporal inhomogeneous, glow to streamer to surface discharge transitions. Plasma Sources Sci Technol. 2023; 32(10): 105016. http://doi.org/10.1088/1361-6595/ad0430

[68] Kogelschatz U. Dielectric-barrier discharges: Their history, discharge physics, and industrial applications. Plasma Chem Plasma Process. 2003; 23(1): 1-46. http://doi.org/10.1023/A:1022470901385

[69] Opaits DF, Shneider MN, Miles RB, Likhanskii AV, Macheret SO. Surface charge in dielectric barrier discharge plasma actuators. Phys Plasmas. 2008; 15(7): 073505. http://doi.org/10.1063/1.2955767

[70] Akishev Y, Aponin G, Balakirev A, Grushin M, Karalnik V, Petryakov A, *et al*. "Memory" and sustention of microdischarges in a steady-state DBD: Volume plasma or surface charge? Plasma Sources Sci Technol. 2011; 20(2): 024005. http://doi.org/10.1088/0963-0252/20/2/024005

[71] Kourtzanidis K, Dufour G, Rogier F. Self-consistent modeling of a surface AC dielectric barrier discharge actuator: In-depth analysis of positive and negative phases. J Phys D Appl Phys. 2020; 54(4): 045203. http://doi.org/10.1088/1361-6463/abbcfd

[72] Yoon SY, Jeon H, Yi C, Park S, Ryu S, Kim SB. Mutual interaction between plasma characteristics and liquid properties in AC-driven pin-to-liquid discharge. Sci Rep. 2018; 8(1): 12037. http://doi.org/10.1038/s41598-018-30540-4

[73] Kawamoto H, Umezu S. Electrohydrodynamic deformation of water surface in a metal pin to water plate corona discharge system. J Phys D Appl Phys. 2005; 38(6): 887-94. http://doi.org/10.1088/0022-3727/38/6/017

[74] Gromov M, Kamarinopoulou N, De Geyter N, Morent R, Snyders R, Vlachos D, *et al*. Plasma-assisted nitrogen fixation: The effect of water presence. Green Chem. 2022; 24(24): 9677-89. http://doi.org/10.1039/D2GC03063B

[75] Vanraes P, Nikiforov A, Bogaerts A, Leys C. Study of an AC dielectric barrier single micro-discharge filament over a water film. Sci Rep. 2018; 8(1): 10919. http://doi.org/10.1038/s41598-018-29189-w

[76] Dimitrakellis P, Faubert F, Wartel M, Gogolides E, Pellerin S. Plasma surface modification of epoxy polymer in air DBD and gliding arc. Processes. 2022; 10(1): 104. http://doi.org/10.3390/pr10010104

[77] Gazeli K, Svarnas P, Lazarou C, Anastassiou C, Georghiou GE, Papadopoulos PK, *et al*. Physical interpretation of a pulsed atmospheric pressure plasma jet following parametric study of the UV-to-NIR emission. Phys Plasmas. 2020; 27(12): 123503. http://doi.org/10.1063/5.0031065

[78] Bruggeman P, Brandenburg R. Atmospheric pressure discharge filaments and microplasmas: Physics, chemistry and diagnostics. J Phys D Appl Phys. 2013; 46(46): 464001. http://doi.org/10.1088/0022-3727/46/46/464001

[79] Bruggeman PJ, Kushner MJ, Locke BR, Gardeniers JGE, Graham WG, Graves DB, *et al*. Plasma-liquid interactions: A review and roadmap. Plasma Sources Sci Technol. 2016; 25(5): 053002. http://doi.org/10.1088/0963-0252/25/5/053002

[80] Locke BR, Shih KY. Review of the methods to form hydrogen peroxide in electrical discharge plasma with liquid water. Plasma Sources Sci Technol. 2011; 20(3): 034006. http://doi.org/10.1088/0963-0252/20/3/034006

[81] Shen J, Cheng C, Xu Z, Lan Y, Ni G, Sui S. Principles and characteristics of cold plasma at gas phase and gas-liquid phase. In: Ding T, Cullen PJ, Yan W, Eds. Applications of Cold Plasma in Food Safety. Singapore: Springer; 2022, p. 1-36. http://doi.org/10.1007/978-981-16-1827-7_1

[82] Bradu C, Kutasi K, Magureanu M, Puač N, Živković S. Reactive nitrogen species in plasma-activated water: Generation, chemistry and application in agriculture. J Phys D Appl Phys. 2020; 53(22): 223001. http://doi.org/10.1088/1361-6463/ab795a

[83] Zhang Z, Shen J, Cheng C, Xu Z, Xia W. Generation of reactive species in atmospheric pressure dielectric barrier discharge with liquid water. Plasma Sci Technol. 2018; 20(4): 044009. http://doi.org/10.1088/2058-6272/aaa437

[84] Cadorin BM, Tralli VD, Ceriani E, Benetoli LOB, Marotta E, Ceretta C, *et al*. Treatment of methyl orange by nitrogen non-thermal plasma in a corona reactor: The role of reactive nitrogen species. J Hazard Mater. 2015; 300: 754-64. http://doi.org/10.1016/j.jhazmat.2015.08.009

[85] Benetoli LOB, Cadorin BM, Postiglione CDS, Souza IG, Debacher NA. Effect of temperature on methylene blue decolorization in aqueous medium in electrical discharge plasma reactor. J Braz Chem Soc. 2011; 22: 1669-78. http://doi.org/10.1590/S0103-50532011000900008

[86] Lukes P, Dolezalova E, Sisrova I, Clupek M. Aqueous-phase chemistry and bactericidal effects from an air discharge plasma in contact with water: Evidence for the formation of peroxynitrite through a pseudo-second-order post-discharge reaction of H2O2 and HNO2. Plasma Sources Sci Technol. 2014; 23(1): 015019. http://doi.org/10.1088/0963-0252/23/1/015019

[87] Cheng X, Liang L, Ye J, Li N, Yan B, Chen G. Influence and mechanism of water matrices on H2O2-based Fenton-like oxidation processes: A review. Sci Total Environ. 2023; 888: 164086. http://doi.org/10.1016/j.scitotenv.2023.164086

[88] Sun F, Liu H, Wang H, Shu D, Chen T, Zou X, *et al*. A novel discovery of a heterogeneous Fenton-like system based on natural siderite: A wide range of pH values from 3 to 9. Sci Total Environ. 2020; 698: 134293. http://doi.org/10.1016/j.scitotenv.2019.134293

[89] Vallés I, Moreno-Andrés J, Sciscenko I, Santos-Juanes L, Arques A. Application of photo-Fenton process to highly saline water matrices: Effect of inorganic ions on iron speciation. Molecules. 2026; 31(1): 56. http://doi.org/10.3390/molecules31010056

[90] Mohseni-Bandpei A, Ghasemi SM, Eslami A, Rafiee M, Sadani M, Ghanbari F. Degradation of atenolol by CuFe2O4/visible light/oxidant: Effects of electron acceptors, synergistic effects, degradation pathways, and mechanism. J Photochem Photobiol A Chem. 2021; 418: 113425. http://doi.org/10.1016/j.jphotochem.2021.113425

[91] Bolton JR, Bircher KG, Tumas W, Tolman CA. Figures-of-merit for the technical development and application of advanced oxidation technologies for both electric- and solar-driven systems (IUPAC Technical Report). Pure Appl Chem. 2001; 73(4): 627-37. http://doi.org/10.1351/pac200173040627

[92] Kim HJ, Lee D, Han S, Lee JC, Kim HW. Degradation pathways and energy efficiency on non-thermal plasma for sulfonamide antibiotics removal: A comparative study. Processes. 2026; 14(8): 1312. http://doi.org/10.3390/pr14081312

[93] Wang J, Zhuan R. Degradation of antibiotics by advanced oxidation processes: An overview. Sci Total Environ. 2020; 701: 135023. http://doi.org/10.1016/j.scitotenv.2019.135023

[94] Martini J, Ighalo JO, Emenike EC, Georgin J, Carissimi E. Degradation of the antibiotic sulfamethoxazole by ozonation: A comprehensive review. CleanMat. 2024; 1(1): 16-51. http://doi.org/10.1002/clem.14

[95] Tang G, Chen Y, Lin S, Li X. The photo- and microbial degradation kinetics and pathways of sulfadoxine in seawater elucidated by liquid chromatography coupled with time-of-flight mass spectrometry. Chemosphere. 2024; 351: 141225. http://doi.org/10.1016/j.chemosphere.2024.141225

[96] Petsi P, Plakas KV, Bizirtsakis P, Anagnostopoulou K, Moschona A, Lambropoulou D, *et al*. Elimination of the pharmaceutical sulfadoxine by electro-Fenton: Reaction kinetics, oxidation pathway and stability of the electrode. Chemosphere. 2025; 375: 144265. http://doi.org/10.1016/j.chemosphere.2025.144265

[97] Savić SD, Kovačević VV, Stanković DM, Sretenović GB, Vasović TD, Vlahović FŽ, *et al*. Complete degradation of propranolol by a water falling film non-thermal plasma reactor: The effects of input power and plasma gases on transformation pathway. Chem Eng J. 2024; 497: 154685. http://doi.org/10.1016/j.cej.2024.154685

[98] Chen T, Ma J, Zhang Q, Xie Z, Zeng Y, Li R, *et al*. Degradation of propranolol by UV-activated persulfate oxidation: Reaction kinetics, mechanisms, reactive sites, transformation pathways and Gaussian calculation. Sci Total Environ. 2019; 690: 878-90. http://doi.org/10.1016/j.scitotenv.2019.07.034

[99] Zhang Q, Du R, Tan C, Chen P, Yu G, Deng S. Efficient degradation of typical pharmaceuticals in water using a novel TiO2/ONLH nano-photocatalyst under natural sunlight. J Hazard Mater. 2021; 403: 123582. http://doi.org/10.1016/j.jhazmat.2020.123582

[100] European Parliament and the Council of the European Union. Regulation (EC) No. 1272/2008. 2008 Dec 16 (accessed on 2024 Jan 15). Available from: https://eur-lex.europa.eu/legal-content/EL/TXT/?uri=CELEX:32008R1272

[101] Li J, Zhao L, Feng M, Huang CH, Sun P. Abiotic transformation and ecotoxicity change of sulfonamide antibiotics in environmental and water treatment processes: A critical review. Water Res. 2021; 202: 117463. http://doi.org/10.1016/j.watres.2021.117463

[102] Shad A, Li C, Zuo J, Liu J, Dar AA, Wang Z. Understanding the ozonated degradation of sulfadimethoxine, exploration of reaction site, and classification of degradation products. Chemosphere. 2018; 212: 228-36. http://doi.org/10.1016/j.chemosphere.2018.08.050

Supplementary Tables

Table S1: Normalized SDX concentration (C/C_0) for each replicate at each timepoint for the NTP and NTP/Fenton processes, and corresponding p-values from two-tailed unpaired Welch's t-test. N/A = not applicable (no variance at t=0; complete removal at t=45, 60 min).

Time (min)	NTP			NTP/Fenton			t-Test
0	**1**	**1**	**1**	**1**	**1**	**1**	**N/A**
2	0,930599	0,952681	0,960876	0,310345	0,303571	0,288288	5,27E-07
5	0,910095	0,929022	0,892019	0,224138	0,214286	0,198198	7,39E-07
7	0,891167	0,867508	0,868545	0,086207	0,071429	0,081081	9,16E-08
10	0,818612	0,847003	0,798122	0,068966	0,071429	0,045045	1,33E-06
15	0,619874	0,678233	0,605634	0,034483	0,035714	0,036036	1,12E-05
20	0,51735	0,531546	0,516432	0	0	0	4,63E-08
30	0,242902	0,20347	0,219092	0	0	0	4,21E-05
45	0	0	0	0	0	0	N/A
60	0	0	0	0	0	0	N/A

All values normalized to t=0. p-values compare NTP vs NTP/Fenton at each timepoint. Significance threshold: $p < 0.05$.

Table S2: LC-Orbitrap MS/MS data for the identification and structural elucidation of the formed TPs in positive ionization (ESI+).

TP_XX	t_R (min)	Molecular Formula (neutral molecule)	Ionization Mode	Adduct Ion	Elemental Composition (*m/z*)	Theor. Mass	Exp. Mass	RDB	Δ (ppm)	Structure
Sulfadoxine	**1,1**	**$C_{12}H_{14}N_4O_4S$**	**ESI+**	**[M+H]**	**$[C_{12}H_{15}N_4O_4S]^+$**	**311,0809**	**311,0813**	**7,5**	**-1,100**	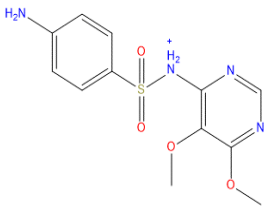
F_1		C5H13N3O4S	ESI+	[M+H]	[C5H14N3O4S]+	212,0700	212,0706	0,5	3,145	
F_2		C4H13N3O3S	ESI+	[M+H]	[C4H14N3O3S]+	184,0750	184,0746	-0,5	-2,491	
F_3		C6H7ON32	ESI+	[M+H]	[C6H8N3O2]+	154,0611	154,0614	4,5	1,863	
F_4		C5H5N3O2	ESI+	[M+H]	[C5H6N3O2]+	140,0455	140,0457	4,5	1,550	
F_5		C4H5N3O	ESI+	[M+H]	[C4H6N3O]+	112,0505	112,0511	3,5	5,458	
F_6		C6H5N	ESI+	[M+H]	[C6H6N]+	92,0495	92,0502	4,5	8,194	
F_7		C5H5N	ESI+	[M+H]	[C5H6N]+	80,0495	80,0503	3,5	1,113	
TP_156	**0,94**	**$C_6H_9N_3O_2$**	**ESI+**	**[M+H]**	**$[C_6H_{10}N_3O_2]$+**	**156,0768**	**156,0771**	**3,5**	**2,415**	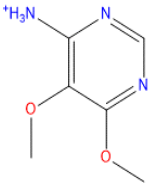
F_1		C4H3N3O2	ESI+	[M+H]	[C4H4N3O2]+	126,0298	126,0304	4,5	2,437	
F_2		C4H5N3O	ESI+	[M+H]	[C4H6N3O]+	112,0505	112,0511	3,5	4,744	
F_3		C3H3N3O	ESI+	[M+H]	[C3H4N3O]+	98,0349	98,0356	3,5	7,667	
F_4		C4H3N3	ESI+	[M+H]	[C4H4N3]+	94,0400	94,0406	4,5	6,872	
F_5		C3H4N2O	ESI+	[M+H]	[C3H5N2O]+	85,0396	85,0403	2,5	8,239	
F_6		C3H6O	ESI+	[M+H]	[C3H7O]+	59,0491	59,0501	0,5	15,556	
TP_247	**0,78**	**$C_{12}H_{14}N_4O_2$**	**ESI+**	**[M+H]**	**$[C_{12}H_{15}N_4O_2]$+**	**247,1190**	**247,1197**	**7,5**	**3,188**	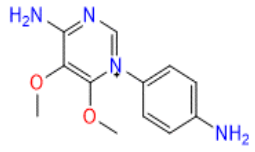
TP_148	**0,80**	**$C_{12}H_{13}N_3O_3$**	**ESI+**	**[M+H]**	**$[C_{12}H_{14}N_3O_3]$+**	**148,1030**	**148,1034**	**7,5**	**1,903**	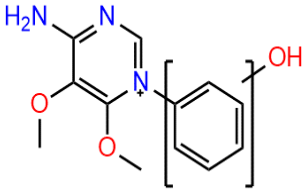
F_1		C10H9N3O2	ESI+	[M+H]	[C10H10N3O2]+	204,0768	204,0771	7,5	1,651	
F_2		C10H6N2O2	ESI+	[M+H]	[C10H7N2O2]+	187,0502	187,0499	8,5	-1,144	
F_3		C8H6N2O	ESI+	[M+H]	[C8H7N2O]+	147,0553	147,0554	6,5	0,752	
F_4		C7H6N2O	ESI+	[M+H]	[C7H7N2O]+	153,0553	135,0557	5,5	2,966	
F_5		C7H5NO	ESI+	[M+H]	[C7H6NO]+	120,0444	120,0449	5,5	3,829	
F_6		C6H7NO	ESI+	[M+H]	[C6H8NO]+	110,0600	110,0608	3,5	6,447	
TP_277	**0,82**	**$C_{12}H_{12}N_4O_4$**	**ESI+**	**[M+H]**	**$[C_{12}H_{13}N_4O_4]$+**	**277,0931**	**277,0935**	**8,5**	**1,366**	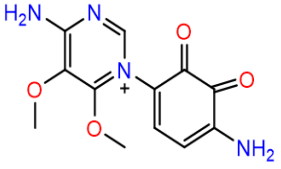
TP_293	**0,81**	**$C_{12}H_{12}N_4O_5$**	**ESI+**	**[M+H]**	**$[C_{12}H_{13}N_4O_5]$+**	**293,0885**	**293,0885**	**8,5**	**1,447**	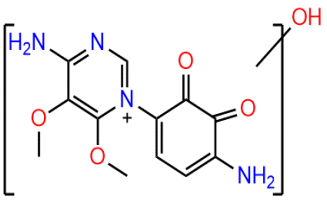
F_1		C11H8N4O5	ESI+	[M+H]	[C11H9N4O5]+	277,0567	277,0572	9,5	1,603	
F_2		C12H11N3O4	ESI+	[M+H]	[C12H12N3O4]+	262,0822	262,0826	8,5	1,326	
F_3		C10H8N4O4	ESI+	[M+H]	[C10H9N4O4]+	249,0618	249,0622	8,5	1,280	
F_4		C10H7N3O3	ESI+	[M+H]	[C10H8N3O3]+	218,0560	218,0567	8,5	2,946	
F_5		C5H5N3O2	ESI+	[M+H]	[C5H6N3O2]+	140,0455	140,0457	4,5	1,407	
F_6		C5H4NO2	ESI+	[M+H]	[C5H5NO2]+	111,0320	111,0319	4,0	4,414	
TP_235	**0,77**	**$C_6H_{10}N_4O_4S$**	**ESI+**	**[M+H]**	**$[C_6H_{11}N_4O_4S]$+**	**235,0496**	**235,0494**	**3,5**	**-0,860**	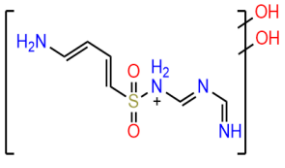

RT: retention time. Molecular formula refers to the neutral compound; adduct ion $[M+H]^+$ used for detection. Mass error calculated as (measured − theoretical)/theoretical × 10^6. TP235 and TP277 are tentatively identified based on accurate mass only; MS^2 fragmentation was not available due to trace-level concentrations.

Table S3: ECOSAR-predicted acute (LC50/EC50) and chronic (ChV) toxicity values (mg/L) for SDX and its transformation products toward fish, daphnid, and green algae. Values represent the most conservative (most toxic) class prediction.

Compound	ECOSAR Class	Fish		Daphnid		Green Algae	
		LC50 (mg/L)	ChV (mg/L)	LC50 (mg/L)	ChV (mg/L)	EC50 (mg/L)	ChV (mg/L)
SDX	Anilines	967	24.4	12.1	0.12	46.4	32.0
TP156	Neutral Organics	7.53×10^{6}	4.13×10^{5}	2.62×10^{6}	6.53×10^{4}	2.57×10^{5}	2.26×10^{4}
TP235	Aliphatic Amines	1.83×10^{5}	7.48×10^{4}	1.15×10^{4}	510	3.37×10^{4}	7060
TP247	Anilines	564	13.1	8.51	0.086	31.5	19.9
TP248	Phenol Amines	22.1	0.183	1.35	0.289	3.25	0.524
TP277	Anilines	2680	92.2	16.8	0.155	73.5	69.2
TP293	Phenol Amines	115	0.693	3.10	0.724	12.7	1.79

ChV: Chronic Value (geometric mean of NOEC and LOEC). LC50/EC50: concentration causing 50% mortality/effect. Lower values indicate higher toxicity.